Available online at www.sciencedirect.com
SCIENCE DIRECT
Journal of the European Ceramic Society 26 (2006) 3011–3016
www.elsevier.com/locate/jeurceramsoc

Synthesis, structure and properties of doped Bi_2O_3

V. Fruth [a,*], A. Ianculescu [b], D. Berger [b], S. Preda [a], G. Voicu [b], E. Tenea [a], M. Popa [a]

[a] *Romanian Academy, Institute of Physical Chemistry, Spl. Independentei 202, Bucharest 060021, Romania*
[b] *University "Politehnica" Bucharest, str. Polizu 1, Bucharest, Ro-78126, Romania*

Available online 15 March 2006

Abstract

Oxide ion conductors have been increasingly studied for many years because of their application in devices with high economical interest such as solid oxide fuel cells (SOFC), oxygen sensors, dense ceramic membranes for oxygen separation, and membrane reactors for oxidative catalysis. Bismuth oxides present polymorph forms, such as δ-, β- or γ-Bi_2O_3, with great potential for such applications, alone or in combination with other oxides. The present study investigates the influence of selected ions (Fe^{3+}, Sb^{3+}/Sb^{5+}, and Ta^{5+}), introduced as dopant in α-Bi_2O_3 and their effect on the structure and properties of the oxide polymorph forms obtained at high temperature. The molar ratio was Bi_2O_3:M_xO_y 0.95:0.05 where $M = Fe_2O_3$, Sb_2O_3 or Ta_2O_5, respectively.

The structural changes of α-Bi_2O_3 were analysed by powder X-ray diffraction, SEM/EDX analysis and infrared spectroscopy. The structural changes are correlated with bulk ceramic characteristics (density, porosity) and their electrical behaviour versus temperature. The presence of some dopants (antimony and tantalum) on bismuth sites enlarges and enhances the stability of the polymorph forms, which is relevant to potential application.

Keywords: Powders-solid state reaction; X-ray methods; Electrical properties; Fuel cells; Substituted Bi_2O_3

1. Introduction

Solid oxide electrolytes and mixed ionic-electronic conductors present great interest for numerous technological applications such as sensors of various types, solid oxide fuel cells (SOFCs), and ceramic membranes for high-purity oxygen separation and partial oxidation of hydrocarbons[1,2]. Among oxygen ion-conducting materials, oxide phases derived from Bi_2O_3 deserve special emphasis owing to their high ionic conductivity with respect to other well-known solid electrolytes[2]. Examples of such phases are stabilised δ-Bi_2O_3, having fluorite-type structure with a very high level of deficiency in the oxygen sublattice and γ-$Bi_4V_2O_{11}$ (the so-called BIMEVOX series), which belongs to the Aurivillius series. At the same time, Bi_2O_3-based materials possess a number of specific disadvantages, including excessively high thermal expansion coefficient (TECs), thermodynamic instability and low mechanical strength.

Bismuth (III) oxide forms two thermodynamically stable polymorph modifications, namely the monoclinic α-phase and the fcc (face-centred cubic) δ-phase[3–8]. The α → δ transition occurs at 978–1013 K. The variation of the transition temperature in such a wide range is related to the purity of samples, their thermal pre-history and oxygen stoichiometry. Cooling down of the high-temperature δ-phase is accompanied by a large hysteresis, when formation of an intermediate metastable tetragonal β-phase and a bcc γ-polymorph (silenite phase) may occur. The metastability of the β and γ phases is determined by an excessive long cation–cation distances in the lattice, since the chemical bonds in bismuth oxide compounds are formed not only between O and Bi ions, but also between bismuth pairs[9]. Therefore, appropriate doping may lead to shorter Bi–Bi distances, stabilizing these phases down to lower temperatures.

In order to better understand how different dopants affect structural stability and conductivity, the behaviour of several (Fe, Ta, or Sb)-doped Bi_2O_3's were investigated. As the radius of the dopant cation becomes smaller, the rate of the conductivity degradation becomes faster[10]. Stereochemical considerations suggest a way to design new oxide-ion conductors: starting from a mixture of oxides, including a lone-pair element (like Tl^+, Ge^{2+}, Sn^{2+}, Pb^{2+}, Sb^{3+}, Bi^{3+}, Se^{4+}, I^{5+} ...) and substituting the lone-pair element by a non-lone-pair element of the same size

* Corresponding author.
E-mail address: vfruth@icf.ro (V. Fruth).

0955-2219/$ – see front matter © 2006 Elsevier Ltd. All rights reserved.
doi:10.1016/j.jeurceramsoc.2006.02.019

and oxidation state. For each two substituted cations, this would create one extra oxygen and one vacancy, which is a favourable situation for oxygen diffusion. As far as possible, the counter-cation should support a variation of co-ordination[11]. The ideal fluorite structure is cubic with the oxide ions in tetrahedral sites and cations at fcc lattice sites. Contact between all ions occurs for an ideal R+/R− ratio equal to 0.732. The SFV (specific free volume-which represents the fraction of the unit cell volume not occupied by the atoms) is 0.50 for δ Bi_2O_3 structure. The Bi^{3+}(VI) radius (0.103 nm) fits well the R+/R− criteria (0.746 compared with the ideal value 0.732). Dopants with smaller ionic radii (<5% mole ratio) should not have significant affect on this structural criterion. From the oxidation state point of view, the best conductivity for stabilised materials is obtained when using 3+ cations[2]. The conductivity also decreases with increasing the dopant concentration, as does the fcc phase stability.

The dopants were selected with respect to several factors: Sb_2O_3 was chosen because Sb^{3+} ($5s^2$) has a similar outermost orbital to Bi^{3+}($6s^2$), being an ionic oxide with very high polarizability[12], Ta_2O_5 was employed as an dopant[11] which is interesting for future work considering the Sr–Bi–Ta–O system. In addition, it was necessary to employ Fe_2O_3 in order to get more insight into the influence of impurities introduced by iron contamination and investigate the Bi rich part of the Bi–Fe–O system.

2. Experimental procedure

Bi_2O_3 (Fluka 99%) and Sb_2O_3 (Merck 99%) Fe_2O_3 (Merck 99%) and Ta_2O_5 (Merck 99%) were mixed in stoichiometric proportions to form $Bi_{1.9}M_{0.1}O_x$ (M = Fe, Sb or Ta) mixtures. The samples were repeatedly ground in a mortar and paste to remove any agglomerates present, then pressed into discs of 10 mm diameter, sintered at different temperatures up to 850 °C and cooled in the furnace till room temperature.

The structure of the obtained materials was determined by X-ray diffraction (XRD). The XRD patterns were recorded with a standard D5000 Siemens Diffractometer $\theta - 2\theta$ equipped with a graphite monochromator, using Cu Kα radiation (λ = 1.5405 Å) operating at 40 mA and 40 kV. IR spectra were recorded using a Specord M80 type Carl Zeiss Jena spectrometer in the spectral range of 2200–400 cm^{-1}. Thermal analysis (DTA/TG) was realized with a MOM-OD 102 derivatograph, in non-isothermal conditions, in air. The powder morphology was determined by scanning electron microscopy with a Scanning microscope Zeiss DSM 942 equipped with a Link Energy Dispersive X-ray system.

3. Results and discussions

The DTA/TG analyses of the starting mixture were carried out in non-isothermal conditions. Table 1 summarise data collected from the three analysed compositions in the temperature range 20–1000 °C; these are correlated with microscopic observation at high temperatures.

The presence of Fe_2O_3 does not modify the polymorph transition temperature (α → δBi_2O_3) but lower the melting point to 802 °C. A different behaviour can be noticed in the case of the other dopants; both increase the melting point of the mixture in Sb<Ta order. A small weight loss (∼1%) was detected on the TG data.

Some remarks can be made on the Sb doped samples: (I) a small exothermal event, associated with the oxidation of Sb^{3+} to Sb^{5+} occurs at 520 °C; (ii) in the temperature range of 520–560 °C, TG curves recorded a weigh loss (1.5%) associated with an endothermic event on the DTA. On cooling, the melts crystallised at 822 °C (undoped sample) and 790–795 °C in the presence of Sb_2O_3. The δ → αBi_2O_3 transition was observed at 660 °C (Bi_2O_3) assigned to the observed exothermal event[13]. When dopants are present, small exothermal events

Table 1
DTA/TG data for oxide mixtures and microscopic observations

Oxide mixture	Thermal events (DTA curve) (°C)	Mass		Microscopic observation
		Increase (%)	Loss (%)	
Bi_2O_3	**733**[c]; 810; 872	0.6 95–411 °C	0.6–0.34 414–900 °C	840 °C—start melting 860 °C—melt very fast
0.95(Bi_2O_3):0.05(Fe_2O_3)	**736**[c]; 790[a]; **802**[c]	1.13 88–932	– 	580 °C—a small contraction in width 750 °C—contraction in high and become more visible at 760 °C 790–800 a hemisphere formation followed by instant melting
0.95(Bi_2O_3):0.05(Sb_2O_3)	520[b]; 550[a]; 560; **735**[c], **878**[c]	0.1 434–525 °C	1.5 520–560	780–790 °C—the surfaces become smoother 870–880 °C the beginning of the melting. At 890 °C the process become very fast
0.95(Bi_2O_3):0.05(Ta_2O_5)	720[a]; **737**[c]; **920**[c]	1 90–410 °C	–	680 °C—a very weak contraction, which increases in intensity at 720 °C, the shape of the samples remaining, unchanged 900–920 °C the samples begin to melt, at 900 °C big micro creaks can be observed after which the sample vanish

[a] Inflexion.
[b] Exothermal event.
[c] Main effects on DTA curve.

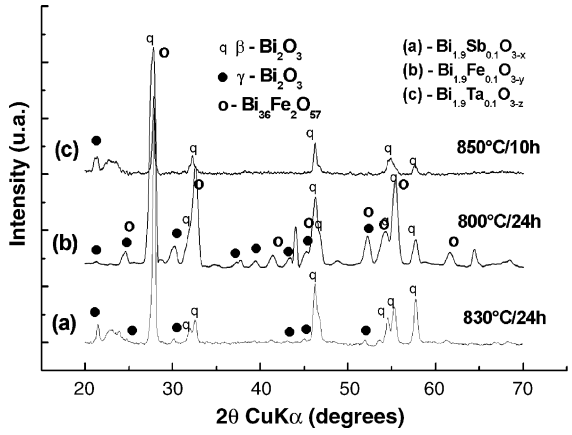

Fig. 1. XRD patterns of the powders with different substitutes and annealing treatments.

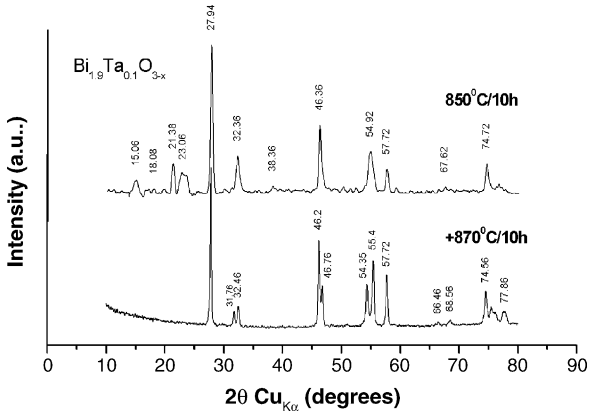

Fig. 2. XRD patterns of the Ta doped Bi_2O_3 powders annealed at two temperatures.

were observed in the range 630–550 °C. The microscopic observations at high temperatures were in good agreement with the DTA data.

Fig. 1 shows a series of XRD patterns of $Bi_{1.9}M_{0.1}O_{3-x}$ solid solution obtained after different annealing treatments. All the samples contained a mixture of phases, β*Bi_2O_3 the main phase (β-Bi_2O_3 type phase) and γ*Bi_2O_3 (γ-Bi_2O_3 type phase) designated tetragonal and cubic (a>10Å) phases, respectively. According to Fries et al.[14] when the contents of the guest oxides were very low, a metastable high temperature phase, was produced, which can be derived as the $\sqrt{2} \times \sqrt{2} \times 1$ superstructure from δ-Bi_2O_3. This observation was confirmed only in the Ta-doped Bi_2O_3 case annealed at 870 °C. All the other cases (β*Bi_2O_3) indicated superstructures with $2 \times 2 \times 1$ relationships to δ-Bi_2O_3 (see Table 2). The cell parameters exhibit small variation for *a* and *b,* in the following order Ta < Fe < Sb and Sb < Ta < Fe for *c* parameter.

The cubic γ*Bi_2O_3 phase is a mixture of phases with the cell parameter in the range 10.08–10.26 Å. These values are influenced by the dopant content and the annealing temperature. This infers a substitution of the Bi^{3+} – 1.03Å – CN6[15] (CN-coordination number) ion by smaller ions (solid solution). The presence of the cubic phase (γ-Bi_2O_3 based type), in small quantities, can be related to the presence of a liquid phase in the system, inferring that this phase crystallised from the melt on cooling. This explains why this phase is almost absent in Ta doped samples. Additional annealing (870 °C for 10 h) produced well crystallised β*Bi_2O_3 phase (Fig. 2) and a trace of another tetragonal phase having a *c* parameter tree times larger than that of the reference (δ-Bi_2O_3). Traces of specific binary compounds, especially Bi rich phases of silenite type, were also observed.

Infrared (IR) spectra have been obtained for the annealed (800 °C/20 h) compositions $Bi_{1.9}M_{0.1}O_x$, where M = Fe, Sb or Ta, at room temperature. The spectra are consistent with the XRD observations. In the case of bismuth sesquioxide the large distortion of the Bi–O polyhedra for α-Bi_2O_3 caused separation of the Bi–O stretching modes into more localised and narrow-line vibrations (dotted line in Fig. 3). The differences in the bond lengths in Bi_2O_3 led to different absorption bands, so it can be assumed that the observed fine structure bands can be correlated with the clusters of similar bond lengths[16]. The characteristic vibrations of the monoclinic Bi_2O_3 structure are slightly shifted and, more significantly, new absorption bands are observed for

Table 2
Structural data for the phases obtained in the doped samples

Sample	Annealing treatments (°C/h)	Identified phases	Space group (SG)	Cells parameters			JCPDS number
				a (Å)	*b* (Å)	*c* (Å)	
$Bi_{1.9}Fe_{0.1}O_{3-x}$	800/20	β*-Bi_2O_3	*P*4*b*2(117)	10.95	10.95	5.629	29-0236
		γ*- Bi_2O_3	*I*23(197)	10.086	10.086	10.086	74-1375
		$Bi_{36}Fe_2O_{57}$	*I*23(197)	10.187	10.187	10.187	42-0183
	Few lines→	δ*-Bi_2O_3	*Pn*3*m*(224)	5.525	5.525	5.525	74-1373
	Trace→	$Bi_2Fe_4O_9$	*Pbam*(55)	7.940	9.440	6.010	42-0181
$Bi_{1.9}Sb_{0.1}O_{3-x}$	830/20	β*-Bi_2O_3	*P*4*b*2(117)	10.956	10.956	5.585	29-0236
		γ*-Bi_2O_3	*I*23(197)	10.0740	10.0740	10.074	74-1375
	Few lines→	δ*-Bi_2O_3	*Pn*3*m*(224)	5.525	5.525	5.525	74-1373
$Bi_{1.9}Ta_{0.1}O_{3-x}$	850/10	β*-Bi_2O_3	*P*4*b*2(117)	10.947	10.947	5.623	29-0236
		γ*-Bi_2O_3	*I*23(197)	10.089	10.089	10.089	74-1375
	Trace→	$Bi_{7.9}Ta_{0.2}O_{12.2}$	*P*421*c*(119)	7.722	7.722	5.646	43-0451
	Few lines→	δ*-Bi_2O_3	*Pn*3*m*(224)	5.525	5.525	5.525	74-1373
	+870/10	β*-Bi_2O_3	*P*421*c*(114)	7.736	7.736	5.604	78-1793

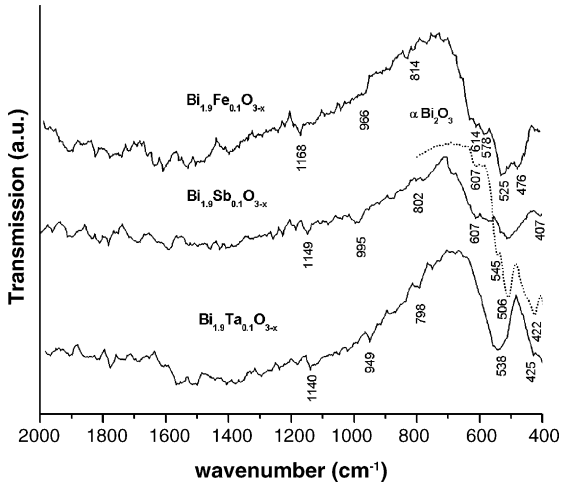

Fig. 3. IR spectra of $Bi_{1.9}M_{0.1}O_{3-x}$ powders where M = Fe, Sb or Ta, after annealing treatment at 800 °C/20 h. Dot line represent IR spectra of α-Bi_2O_3.

all the M-doped samples (Fig. 3). A systematically shift of the bands towards higher wavenumber was observed, suggesting a possible substitution of Bi^{3+} by the smaller ions. Changing the substituted ion in the samples led to different features in the IR spectra. For Ta doped samples two broad absorption bands were observed (400–470 cm^{-1} and 470–640 cm^{-1}), being different in comparison with the starting oxides. Fe doped samples present some similarity with the Bi_2O_3 IR-spectra[16] inferring different formation mechanism. A common vibration (520, 540 and 560 for Fe, Ta and Sb doped samples), characteristic of cubic silenite type structure was identified. The difference between doped samples can be explained by the multiphase composition of the samples as confirmed by the XRD data. It can be concluded that the broad envelope in the metal-oxygen stretching region in the IR spectra of the doped phases can be associated with highly polar bonds.

The SEM images underlined the influence of the substituted oxide on the morphology of samples (exemplified by the sample annealed at two different temperatures). Significant differences may be noticed. Most of the samples present two phases, one well formed with large particles (>10 μm). In the case of Fe doped samples the dimensional homogeneity of the sample was lower than in the other cases. Two main ranges of granules may be observed, 5–10 μm and greater than 30 μm. Reduced porosity and good chemical homogeneity may be observed (Fig. 4).

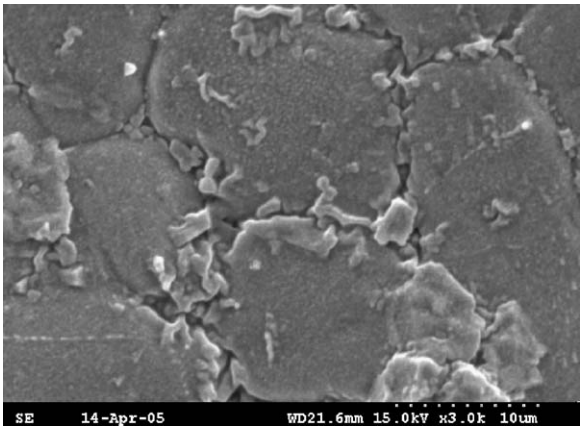

Fig. 4. SEM image of $0.95(Bi_2O_3)$:$0.05(Fe_2O_3)$ composition after 20 h annealing treatment at 800 °C, in air.

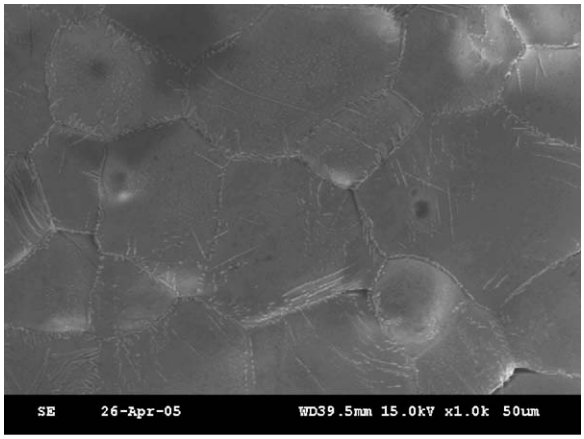

(a)

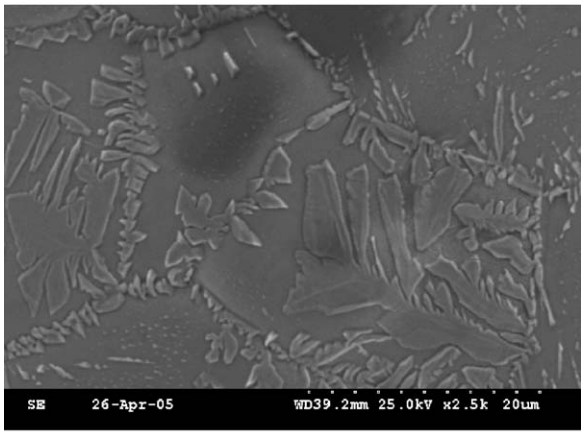

(b)

Fig. 5. SEM images of $0.95(Bi_2O_3)$:$0.05(Sb_2O_3)$ composition after 10 h annealing treatment at 830 °C, in air, at different magnitudes: ×1.0 k (a), ×2.5 k (b).

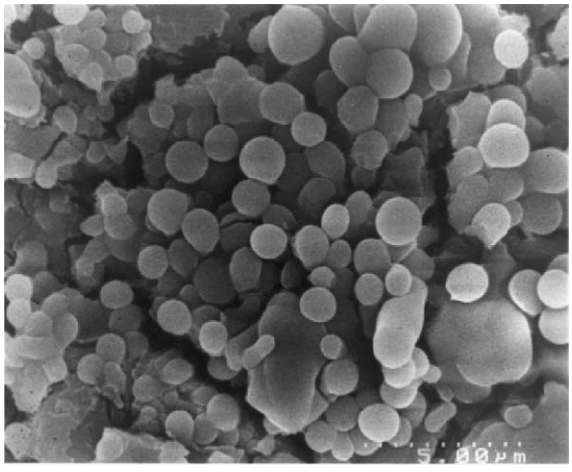

Fig. 6. Fig. SEM image of $0.95(Bi_2O_3)$:$0.05(Sb_2O_3)$ composition after 20 h annealing treatment at 820 °C, in air.

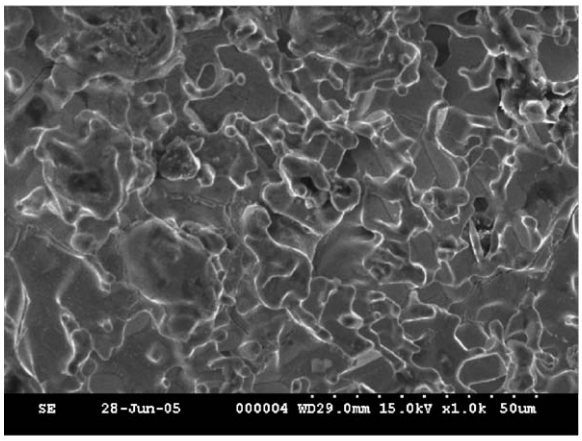

(a)

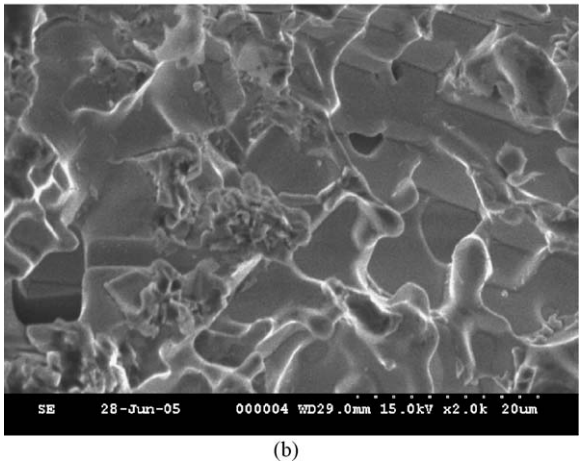

(b)

Fig. 7. SEM images of $0.95(Bi_2O_3)$:$0.05(Ta_2O_5)$ composition after 10 h annealing treatment at 850 °C, in air (a) and additional 870 °C/10 h treatment of the same sample (b).

In antimony-doped samples, annealed at 830 °C/20 h, a homogenous microstructure composed of large granules (∼50 μm) with well-defined polygonal boundaries was obtained (Fig. 5a). The porosity is not present in the inter-granular area. Two phases are present; the second one (needle shape Fig. 5b) can be attributable to a metastable γ* type bismuth oxide phase. A good dispersion of the atom species was achieved.

An interesting fact concerns the conditions under which the grain boundary liquid phase occurred. This is well below the eutectic temperature as determined by DTA. One can presume that the substituted oxide (Fe_2O_3, Sb_2O_3 or Ta_2O_5) forms a thin coating on the surface of Bi_2O_3 powder particles during heating. It is also well known that the melting point of materials decreases with decreasing particle size[17,18]. One has to distinguish between surface melting and melting of small particles below the melting temperature of the bulk. However, both scale with $T_m(D) = T_m(\infty) - a/Z$ formula, where $T_m(\infty)$ is the bulk melting temperature, Z the particle diameter or layer thickness and a is a constant. These considerations are in good agreement with the SEM images and observation of high temperature microscopy. The boundary and surface liquid phase explain both the sample shrinkage at lower temperature and the very good connection between grains after sintering. In the case of Sb doped samples this mechanism is better evidenced. Fig. 6 shows an SEM image of the Sb doped samples, thermal annealed at 820 °C for 20 h. One may distinguish two phases; one with polyhedral shape, tens of microns in size, close to the starting composition ($Bi_{1.78}Sb_{0.22}O_3$), and the other nanometric droplets of increased antimony content ($Bi_{1.42}Sb_{0.58}O_3$). The spherical particles are located on the surface of the larger particles. From this phase a needle shape phase crystallised (Fig. 5b) which is localised at the grain junctions.

A different process occurred for Ta doped samples. The observed grains (Fig. 7a) present curved edges at 850 °C and a very good connection after sintering at 870 °C, without any porosity (Fig. 7b).

Electrical conductivity as a function of temperature data exhibits almost the same profiles, with a trend that is typical for a solid electrolyte (Fig. 8). At lower temperatures (up to 200 °C) only an extrinsic mechanism can be noticed with a small tendency to increase in the Fe doped samples. As the temperature increase the intrinsic conduction became predominant and two slopes can be identified. The high values for the Ta doped samples can be explained by a mixed conduction mechanism, ionic and electronic (n type). The conductivity increases in the order Fe < Sb < Ta.

Table 3 shows the bulk properties, densities and shrinkage, obtained with different annealing treatment. The results

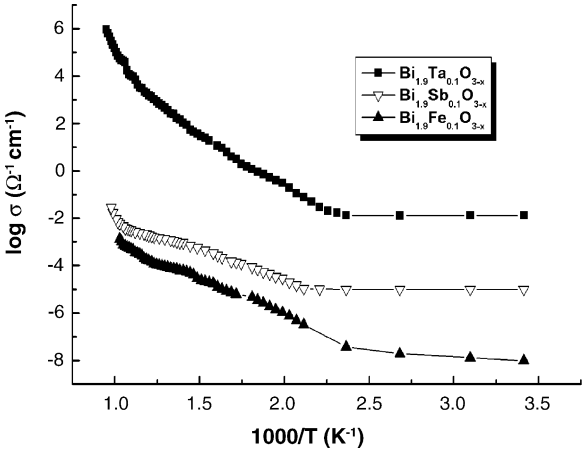

Fig. 8. Temperature dependence of the total electrical conductivity, in air.

Table 3
Densities and shrinkage of the ceramic bodies at different temperatures

	Ionic radii (nm)	Thermal treatment	Shrinkage[a] (%)	Density (g/cm^3)
$Bi_{1.9}Ta_{0.1}O_x$	Ta^{5+}-0.064	800 °C/20 h	17.20	7.77
		850 °C/10 h	8	8.95
		+870 °C/10 h	5.8	9.2
$Bi_{1.9}Sb_{0.1}O_x$	Sb^{3+}-0.08	800 °C/20 h	9.5	8.46
	Sb^{5+}-0.06	830 °C/10 h	5.7	8.86
$Bi_{1.9}Fe_{0.1}O_x$	Fe^{3+}-0.064	800 °C/2 h	1.3	8.62
Bi_2O_{3-x}	Bi^{3+}-0.103	800 °C/2 h	9.6	8.08

[a] Defined as $100((\Phi - \Phi_0)/\Phi_0)$ where Φ is final diameter.

are in accordance with SEM observations and theoretical considerations. The densities increase as the annealing temperature increase. Good sintered bodies, with high densities were obtained. It may be noted that the shrinkage is dependent on the ionic radius of the dopant.

4. Conclusions

The influence of three dopants (Fe_2O_3, Sb_2O_3 or Ta_2O_5 at 5% mole level) on microstructure and properties of thermal treated Bi_2O_3 were investigated. The nature of the dopants influenced the behaviour of the staring mixtures in non-isothermal conditions; Sb_2O_3 and Ta_2O_5 enlarged the stability domain of the δ-Bi_2O_3 phase. The melting point of Ta doped Bi_2O_3 is over 900 °C.

The phases present in the annealed samples consist of a major one, with tetragonal symmetry, and a second one with cubic symmetry, localised especially in the boundary area and related to the presence of the liquid phase. The changes in the IR spectra of all the samples are determined both by the nature of the dopant and the beginning of a new network arrangement, characteristic for metastable Bi_2O_3 polymorph forms.

SEM/EDAX observations indicate well-sintered bodies, supporting the density data. The presence of antimony oxide promotes uniformity of the grains (∼50 μm). Iron oxide produced a less homogenous structure with a wide range of grain sizes.

The electric conductivity is also influenced by the nature of the dopants. The best values were obtained for Ta doped Bi_2O_3 samples; this can be explained by the existence of a mixed conduction mechanism.

The presence of selected dopants (antimony and tantalum) on bismuth sites, enlarged and enhanced the stability of the polymorph forms, which is relevant for potential application.

References

1. Sammes, N. M., Fee, M., Phillips, M. G. and Ratnaraj, R. J., Improved mechanical properties of bismuth lead oxide. *J. Mater. Sci. Lett.*, 1994, **13**(19), 1395–1396.
2. Boivin, J. C., Structural and electrochemical features of fast oxide ion conductors. *Int. J. Inorg. Mater.*, 2001, **3**, 1261–1266.
3. Silen, L. G., X-Ray studies on bismuth trioxide. *Ark. Kemi. Mineral. Geol.*, 1937, **12A**(18), 1–15.
4. Gattow, G. and Schroder, H., Bismuth oxides. III. *Z. Anorg. Allg. Chem.*, 1962, **318**(3-4), 176–189.
5. Levin, E. M. and Roth, R. S., Polymorphism of bismuth sesquioxide. I. *J. Res. Natl. Bur. Stand.*, 1964, **68**, 189–195.
6. Medernach, J. W. and Snyder, R. L., Powder diffraction patterns and structures of bismuth oxides. *J. Am. Ceram. Soc.*, 1978, **61**(No. 11–12), 494–497.
7. Aurivillius, B. and Malmros, G., Crystal structures of β-Bi_2O_3. *Trans. R. Inst. Technol., Stockholm*, 1972, **291**, 545–562.
8. Shuk, P., Wiemhoferb, H.-D., Guth, U., Gijpeld, W. and Greenblatt, M., Oxide ion conducting solid electrolytes based on Bi_2O_3. *Solid State Ionics*, 1996, **89**, 179–196.
9. Kharton, V. V., Naumovich, E. N., Yaremchenko, A. A. and Marques, F. M. B., IV Bismuth oxide-based ceramics. *J. Solid State Electrochem.*, 2001, **5**, 160–187.
10. Jiang, N. and Wachsman, E. D., Structural stability and conductivity of phase-stabilized cubic bismuth oxides. *J. Am. Ceram. Soc.*, 1999, **82**, 3057–3064.
11. Ling, C. D., Withers, R. L., Schmid, S. and Thompson, J. G., A review of bismuth binary oxides in the systems Bi_2O_3-Nb_2O_5, Bi_2O_3-Ta_2O_5, Bi_2O_3-MoO_3 and Bi_2O3-WO_3. *Solid State Chem.*, 1998, **13**, 742–761.
12. Dimitriev, V. and Komatsu, T., Classification of simple oxides: a polarizability approach. *J. Solid State Chem.*, 2002, **163**, 100–112.
13. Fruth, V., Popa, M., Berger, D., Ionica, C. M. and Jitianu, M., Phases investigation in the antimony doped Bi_2O_3 system. *J. Eur. Ceram. Soc.*, 2004, **24**, 1295–1299.
14. Fries, T., Lang, G. and Kammerling-Sack, S., Defect fluorite structures in the Bi-rich part of the system Bi_2O_3-Re_2O_3. *Solid State Ionics*, 1996, **89**, 233–240.
15. Shannon, R. D., Revised effective ionic radii and systematic studies of interatomic distances in halides and chalcogenides. *Acta Cryst.*, 1976, **A32**, 751–767.
16. Betsch, R. J. and White, W. B., Vibrational spectra of bismuth oxide and the sillenite-structure bismuth oxide derivatives. *Spectrochim. Acta*, 1979, **34A**, 505–514.
17. Oxtoby, D. W., New perspectives on freezing and melting. *Nature*, 1990, **347**, 725–730.
18. Chan, R. W., Melting and the surface. *Nature*, 1986, **323**, 668–669.